Feng Gao, Yang Wang, Liang Xu, Zhenhua Feng, Qiong Wu, Baohui Zhang, Jingyao Liu, Jiang Tang, Ming Tang, Huan Liu, Songnian Fu, Yinlan Ruan, Heike Ebendorff-Heidepriem and Deming Liu

Light-controllable fiber interferometer utilizing photoexcitation dynamics in colloidal quantum dot

Optics Express, 2018; 26(4):3903-3914

DOI: http://dx.doi.org/10.1364/OE.26.003903

Research Article | Vol. 26, No. 4 | 19 Feb 2018 | OPTICS EXPRESS 3903
Optics EXPRESS

Light-controllable fiber interferometer utilizing photoexcitation dynamics in colloidal quantum dot

FENG GAO,[1] YANG WANG,[1] LIANG XU,[1] ZHENHUA FENG,[1] QIONG WU,[1] BAOHUI ZHANG,[1] JINGYAO LIU,[1] JIANG TANG,[1] MING TANG,[1,4] HUAN LIU,[1,5] SONGNIAN FU,[1] YINLAN RUAN,[2,3] HEIKE EBENDORFF-HEIDEPRIEM,[2,3] AND DEMING LIU[1]

[1]*Wuhan National Laboratory for Optoelectronics (WNLO) & National Engineering Laboratory for Next Generation Internet Access System, School of Optical and Electronic Information, Huazhong University of Science and Technology, Wuhan 430074, China*
[2]*ARC Centre of Excellence for Nanoscale BioPhotonics, Adelaide, SA 5005, Australia*
[3]*Institute for Photonics and Advanced Sensing, School of Physical Sciences, The University of Adelaide, Adelaide, SA 5005, Australia*
[4]*tangming@mail.hust.edu.cn*
[5]*huan@mail.hust.edu.cn*

Abstract: The development of highly efficient light-controlled functional fiber elements has become indispensable to optical fiber communication systems. Traditional nonlinearity-based optical fiber devices suffer from the demerits of complex/expensive components, high peak power requirements, and poor efficiency. In this study, we utilize colloidal quantum dots (CQDs) to develop a light-controlled optical fiber interferometer (FI) for the all-optical control of the transmission spectrum. A specially designed exposed-core microstructure fiber (ECMF) is utilized to form the functional structure. Two types of PbS CQDs with absorption wavelengths around 1180 nm and 1580 nm, respectively, are deposited on the ECMF to enable the functional FI. The wavelength and power of control light are key factors for tailoring the FI transmission spectrum. A satisfactory recovery property and linear relationship between the spectrum shift and the power of control light at certain wavelength are achieved. The highest wavelength shift sensitivity of our light-controlled FI is 4.6 pm/mW, corresponding to an effective refractive index (RI) change of 5×10^{-6} /mW. We established a theoretical model to reveal that the RI of the CQD layer is governed by photoexcitation dynamics in CQD with the light absorption at certain wavelength. The concentration of charge carriers in the CQD layer can be relatively high under light illumination owing to their small size-related quantum confinement, which implies that low light power (mW-level in this work) can change the refractive index of the CQDs. Meanwhile, the absorption wavelength of quantum dots can be easily tuned via CQD size control to match specific operating wavelength windows. We further apply the CQD-based FI as a light-controllable fiber filter (LCFF) in a 50-km standard single-mode fiber-based communication system with 12.5-Gbps on-off keying direct modulation. Chirp management and dispersion compensation are successfully achieved by using the developed LCFF to obtain error-free transmission. CQDs possess excellent solution processability, and they can be deposited uniformly and conformally on various substrates such as fibers, silicon chips, and other complex structure surfaces, offering a powerful new degree of freedom to develop light control devices for optical communication.

OCIS codes: (160.5320) Photorefractive materials; (230.1150) All-optical devices; (230.5590) Quantum-well, -wire and -dot devices.

#313014 https://doi.org/10.1364/OE.26.003903
Journal © 2018 Received 20 Nov 2017; revised 24 Jan 2018; accepted 30 Jan 2018; published 6 Feb 2018

Optics EXPRESS

References and links

1. R. He, P. J. A. Sazio, A. C. Peacock, N. Healy, J. R. Sparks, M. Krishnamurthi, V. Gopalan, and J. V. Badding, "Integration of gigahertz-bandwidth semiconductor devices inside microstructured optical fibres," Nat. Photonics **6**(3), 174–179 (2012).
2. L. Scolari, T. Alkeskjold, J. Riishede, A. Bjarklev, D. Hermann, A. Anawati, M. Nielsen, and P. Bassi, "Continuously tunable devices based on electrical control of dual-frequency liquid crystal filled photonic bandgap fibers," Opt. Express **13**(19), 7483–7496 (2005).
3. K. Liu, W. C. Jing, G. D. Peng, J. Z. Zhang, D. G. Jia, H. X. Zhang, and Y. M. Zhang, "Investigation of PZT driven tunable optical filter nonlinearity using FBG optical fiber sensing system," Opt. Commun. **281**(12), 3286–3290 (2008).
4. W. Qian, C. L. Zhao, S. He, X. Dong, S. Zhang, Z. Zhang, S. Jin, J. Guo, and H. Wei, "High-sensitivity temperature sensor based on an alcohol-filled photonic crystal fiber loop mirror," Opt. Lett. **36**(9), 1548–1550 (2011).
5. H. K. Tyagi, M. A. Schmidt, L. Prill Sempere, and P. S. J. Russell, "Optical properties of photonic crystal fiber with integral micron-sized Ge wire," Opt. Express **16**(22), 17227–17236 (2008).
6. G. Chesini, V. A. Serrão, M. A. R. Franco, and C. M. B. Cordeiro, "Analysis and optimization of an all-fiber device based on photonic crystal fiber with integrated electrodes," Opt. Express **18**(3), 2842–2848 (2010).
7. X. Yang, Y. Liu, Y. Zheng, S. Li, L. Yuan, T. Yuan, and C. Tong, "A capillary optical fiber modulator derivates from magnetic fluid," Opt. Commun. **304**, 83–86 (2013).
8. R. Normandin, D. C. Houghton, and M. Simard-Normandin, "All-optical, silicon based, fiber optic modulator using a near cutoff region," Can. J. Phys. **67**(67), 412–419 (1989).
9. K. H. Schoenbach, V. K. Lakdawala, R. Germer, and S. T. Ko, "An optically controlled closing and opening semiconductor switch," J. Appl. Phys. **63**(7), 2460–2463 (1988).
10. C. Lee, P. Mak, and A. DeFonzo, "Optical control of millimeter-wave propagation in dielectric waveguides," IEEE J. Quantum Electron. **16**(3), 277–288 (1980).
11. V. R. Almeida, C. A. Barrios, R. R. Panepucci, and M. Lipson, "All-optical control of light on a silicon chip," Nature **431**(7012), 1081–1084 (2004).
12. T. A. Ibrahim, W. Cao, Y. Kim, J. Li, J. Goldhar, P. T. Ho, and C. H. Lee, "All-optical switching in a laterally coupled microring resonator by carrier injection," IEEE Photonics Technol. Lett. **15**(1), 36–38 (2003).
13. H. K. Tsang, C. S. Wong, T. K. Liang, I. E. Day, S. W. Roberts, A. Harpin, J. Drake, and M. Asghari, "Optical dispersion, two-photon absorption and self-phase modulation in silicon waveguides at 1.5 μm wavelength," Appl. Phys. Lett. **80**(3), 416–418 (2002).
14. A. Bogoni, M. Scaffardi, P. Ghelfi, and L. Poti, "Nonlinear Optical Loop Mirrors: Investigation Solution and Experimental Validation for Undesirable Counterpropagating Effects in All-Optical Signal Processing," IEEE J. Sel. Top. Quantum Electron. **10**(5), 1115–1123 (2004).
15. D. Gammon, "Electrons in artificial atoms," Nature **405**(6789), 899–900 (2000).
16. A. P. Alivisatos, "Semiconductor Clusters, Nanocrystals, and Quantum Dots," Science **271**(5251), 933–937 (1996).
17. Z. Ning, O. Voznyy, J. Pan, S. Hoogland, V. Adinolfi, J. Xu, M. Li, A. R. Kirmani, J. P. Sun, J. Minor, K. W. Kemp, H. Dong, L. Rollny, A. Labelle, G. Carey, B. Sutherland, I. Hill, A. Amassian, H. Liu, J. Tang, O. M. Bakr, and E. H. Sargent, "Air-stable n-type colloidal quantum dot solids," Nat. Mater. **13**(8), 822–828 (2014).
18. J. Tang, H. Liu, D. Zhitomirsky, S. Hoogland, X. Wang, M. Furukawa, L. Levina, and E. H. Sargent, "Quantum Junction Solar Cells," Nano Lett. **12**(9), 4889–4894 (2012).
19. L. Ding, C. Fan, Y. Zhong, T. Li, and J. Huang, "A sensitive optic fiber sensor based on CdSe QDs fluorophore for nitric oxide detection," Sens. Actuators B Chem. **185**, 70–76 (2013).
20. R. Tabassum and B. D. Gupta, "Fiber optic hydrogen gas sensor utilizing surface plasmon resonance and native defects of zinc oxide by palladium," J. Opt. **18**(1), 015004 (2016).
21. A. Bozolan, R. M. Gerosa, C. J. S. de Matos, and M. A. Romero, "Temperature Sensing Using Colloidal-Core Photonic Crystal Fiber," IEEE Sens. J. **12**(1), 195–200 (2012).
22. S. C. Warren-Smith, H. Ebendorff-Heidepriem, T. C. Foo, R. Moore, C. Davis, and T. M. Monro, "Exposed-core microstructured optical fibers for real-time fluorescence sensing," Opt. Express **17**(21), 18533–18542 (2009).
23. Y. Rao, M. Deng, D. Duan, and T. Zhu, "In-line fiber Fabry-Perot refractive-index tip sensor based on endlessly photonic crystal fiber," Sens. Actuators A Phys. **148**(1), 33–38 (2008).
24. M. Jiang, Q. Li, J. Wang, W. Yao, Z. Jin, Q. Sui, J. Shi, F. Zhang, L. Jia, and W. Dong, "Optical Response of Fiber-Optic Fabry-Perot Refractive-Index Tip Sensor Coated With Polyelectrolyte Multilayer Ultra-Thin Films," J. Lightwave Technol. **31**(14), 2321–2326 (2013).
25. Y. Ruan, L. Ding, J. Duan, H. Ebendorff-Heidepriem, and T. M. Monro, "Integration of conductive reduced graphene oxide into microstructured optical fibres for optoelectronics applications," Sci. Rep. **6**, 21682 (2016).
26. R. Saran and R. J. Curry, "Lead sulphide nanocrystal photodetector technologies," Nat. Photonics **10**(2), 81–92 (2016).
27. E. H. Sargent, "Infrared Quantum Dots," Adv. Mater. **17**(5), 515–522 (2005).
28. M. Li, D. Zhou, J. Zhao, Z. Zheng, J. He, L. Hu, Z. Xia, J. Tang, and H. Liu, "Resistive gas sensors based on colloidal quantum dot (CQD) solids for hydrogen sulfide detection," Sensors Actuat. B **217**, 198–201 (2015).

Optics EXPRESS

29. H. Liu, M. Li, O. Voznyy, L. Hu, Q. Fu, D. Zhou, Z. Xia, E. H. Sargent, and J. Tang, "Physically Flexible, Rapid-Response Gas Sensor Based on Colloidal Quantum Dot Solids," Adv. Mater. **26**(17), 2718–2724 (2014).
30. M. T. Crisp and N. A. Kotov, "Preparation of nanoparticle coatings on surfaces of complex geometry," Nano Lett. **3**(2), 173–177 (2003).
31. J. M. Luther, P. K. Jain, T. Ewers, and A. P. Alivisatos, "Localized surface plasmon resonances arising from free carriers in doped quantum dots," Nat. Mater. **10**(5), 361–366 (2011).
32. Z. Li, L. Yi, H. Ji, and W. Hu, "100-Gb/s TWDM-PON based on 10G optical devices," Opt. Express **24**(12), 12941–12948 (2016).

1. Introduction

Optical fibers are media that offer the lowest attenuation of light transmission, and hence, they are widely applied in high-speed, large-capacity, and low-latency communication systems. Nowadays, several communication applications require the development of functional fiber elements with regard to energy- and cost-sensitive requirements, for e.g., distributed networks and last-mile communication. The integration of functional materials into silica fibers is a promising approach to develop fiber devices [1]. In this regard, photonic-crystal fiber (PCFs) are considered ideal to provide a suitable microstructure into which functional materials can be "filled." It has been reported that stress, temperature, and electric and magnetic fields can be applied to affect the mode field in PCF integrated with media such as lead zirconate titanate, alcohol, liquid crystals, semiconductors, metals, and magneto-fluids) [2–7]. However, several problems need to be solved in terms of system stabilization and material deposition in these devices. While liquid-phase materials can be easily filled into PCFs, the resulting devices are not robust. Meanwhile, solid materials exhibit great performance and robustness, but it is difficult to deposit such materials in a PCF.

It is attractive to develop all-optical-controllable devices which do not require electrodes, and can be remotely controlled with great flexibility. The development of light-controlled devices can significantly increase the operational freedom of communication systems. Meanwhile, the idea of manipulating the carrier density of semiconductors by light to invent new light-controlled optical devices has been proposed for many decades now [8–10]. However, the fundamental problem is that a reasonable refractive index (RI) change can occur only if the carrier density in the semiconductors is biased to a relatively high level, and therefore, the light used to control the RI must have very high power. Although shrinking the volume of semiconductor materials and employing a pulsed laser as the light controller can somewhat reduce the average optical power (as demonstrated in planar waveguides), the peak power is still too high [11–13]. Meanwhile, nonlinear effects in fibers have been exploited to develop light-controlled fiber devices [14]; however, such devices require the application of watt-level average power to observe a reasonable RI change.

Colloidal quantum dots (CQDs) are zero-dimensional semiconductor materials that can be utilized in the fabrication of fiber devices since they offer several advantages. Firstly, the electrons in a CQD are confined to a very small volume, typically several hundreds to thousands of atoms per particle [15-16]. The concentration of photoexcited electrons can reach a high level with low-power incident light. Secondly, CQDs are highly tunable materials; the fundamental properties of a CQD, including the band gap, carrier lifetime, melting point, and fluorescence wavelength can be tuned by merely altering the CQD size [17, 18]. Thirdly, solution-processed CQDs afford nanoscale dispersion, and thus, the functional material can easily and conformally be deposited on fiber or silicon chips to fabricate robust devices. In this regard, many schemes have been proposed to develop fiber sensors based on the surface plasmonic effect and fluorescence wavelength [19–21]. Meanwhile, the idea of manipulating the photoelectron concentration in CQDs to tune the RI under light application is yet to see further development.

In this study, we investigate the prospect of employing CQD to add light-controlled functionality to fiber. For demonstration purposes, we fabricate a light-controlled fiber interferometer (FI) enabled by CQDs. The light within the CQD absorption wavelength region was applied as the control light and its intensity was utilized to linearly control the

Optics EXPRESS

transmission spectrum of the FI. A specially designed exposed-core microstructure fiber (ECMF) is used to fabricate a FI [22–24]. CQDs with specially chosen absorption wavelengths (1180 nm and 1580 nm) are deposited onto the exposed area of the ECMF to fabricate the FI. When compared with bulk semiconductor materials and silicon chip devices, our device only requires several mW of input light power to induce a significant refractive index change. Three factors are considered as the main reason for the low energy photoexcitation dynamics of CQD in our experiments: (a) the quantum confinement and the small size of the CQD enable high carrier (charge) density, typically 10^{18} ~10^{19} cm^{-3}, at mW light injection; (b) the exposed core enable the near core deposition in the fiber by which the CQD could receive sufficient light energy illumination at the evanescent field [25]; and (c) the evanescent field along the core surface enhances the photoexcitation in CQD. A linear relationship is observed between the wavelength shift and the incident light power, and the highest sensitivity of the light-controlled fiber FI is 4.25 pm/mW. Our results also demonstrate adequate recovery and stabilization properties of the device. For application in communication systems, the CQD-enabled FI is treated as a light-controllable fiber filter (LCFF) in which the control signal is transmitted by light as opposed to electric current in traditional devices; consequently, CQD-based devices are power-efficient and can be used for remote control of communication systems. In this study, a PbS CQD layer with an absorption wavelength of ~1180 nm is used to fabricate the LCFF. The control light wavelength is chosen to be 980 nm, and the transmission light wavelength is 1550 nm. The 1180-nm CQD fcan absorb light at 980 nm, while it is transparent to 1550-nm-wavelength light. The device is then applied in a 12.5-Gbps directly modulated on-off keying (OOK) communication system for 50-km SMF transmission for chirp management and dispersion compensation.

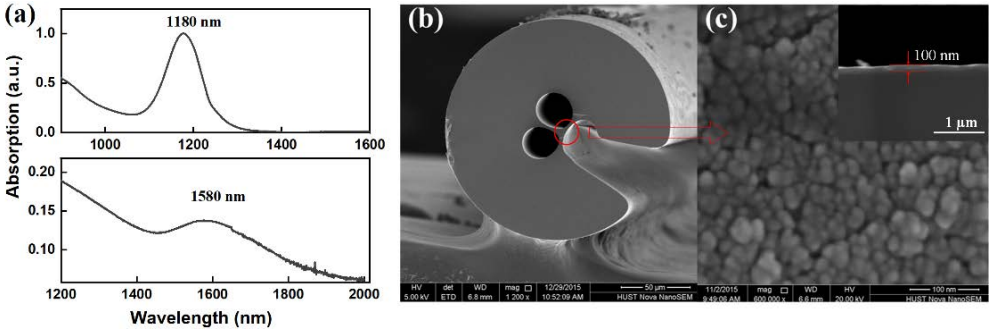

Fig. 1. Characterization of fabricated CQD and fiber structure. (a) Absorption spectra of the two kinds solution-processed PbS CQD as measured by a UV-vis/NIR spectrophotometer. (b) The ECMF cross-sectional image was observed by means of a scanning electron microscope (SEM). (c) SEM image of PbS CQD on the surface of the fiber, the insert was the profile of the CQD layer, the insert image was the profile of the CQD layer, the typical thickness was about 100 nm.

2. Materials and methods

Lead sulfide (PbS) has a bandgap of ~0.41 eV and its exciton Bohr radius is ~18 nm [26]. The strong quantum confinement of PbS quantum dots allows a size-dependent bandgap so that controllable access to different portions of the broad near infrared spectrum could be achieved through variation of synthetic parameters [27]. The PbS CQDs were synthesized by the a hot-injection method [28-29] and dispersed in octane at a concentration of 50 mg/mL. In this work, CQDs with different sizes were fabricated to investigate their optical properties. The absorption spectra of the CQDs utilized in the experiment were measured by means of a UV-vis/NIR spectrophotometer. The absorption wavelengths were ~1180 nm and ~1580 nm for two different CQD sizes of 4.04 nm and 6.09 nm, respectively, as illustrated in Fig. 1(a).

The ECMF was employed to facilitate the deposition of nanomaterial around the fiber core. The profile of the fiber was observed by means of a scanning electron microscope

Optics EXPRESS

(SEM) Fig. 1(b). From the figure, we note that three large air holes surround the fiber center, with one of them exposed to the external environment. The core diameter of the ECMF is about 6 μm. The air hole is an approximate ellipse. The long axis is about 30 μm while the short axis is about 24 μm [22]. The ECMF-based FI was fabricated as follows: (a) The ECMF was carefully cleaved such that its structure was not destroyed; (b) the ECMF was spliced with a single-mode fiber (SMF) by means of low charge splicing under the help of a fusion splicer (Fujikura, FSM-60s); (c) The ECMF was cut to leave a 3.4-mm length between the splicing point and the ECMF ending. A phase delay occurred between the light reflected at the splicing point and the light reflected at the ECMF end. Interference was observed between the two beams of light, with the free spectral range (FSR) being ~2.3 nm, corresponding to the length of the ECMF.

The ECMF was carefully cleaned via ultrasonic processing and then treated with methyl alcohol for 20 min. Subsequently, CQDs were conformally deposited on the fiber device via the layer-by-layer dip coating method [30]. The SEM was used to characterize the dispersion of the CQDs on the fiber; the corresponding SEM image is shown in Fig. 1(c). The CQDs were successfully deposited on the ECMF and dispersed uniformly over a scale of several hundred nanometers in the open core of the PCF. The thickness of the CQD layer was expected to be thick to enhance the light control efficiency. However, a thicker layer will also decrease the extinction ratio of the FI. The typical thickness of the layer was about 100 nm observed from the insert image of Fig. 1(c) and it was an optimized parameter after continuous experiments.

Our experimental setup is illustrated in Fig. 2. The source light was a broadband light (BBL) source (Amonics) with an output ranging from 1525 to 1575 nm, with the output light transmitted through an optical circulator (OC) and wavelength division multiplexer (WDM) (or a coupler) before arriving at the FI. The WDM was applied for beam combination for the 980 nm single wavelength laser and BBL while the coupler was used for 1550 nm laser. At the FI, the incident light was reflected by the ECMF and coupled back to an optical spectrum analyzer (OSA, Yokogawa AQ6370C). The BBL generated the basic optical spectrum of the FI, and the spectrum was recorded by the OSA. A single-wavelength laser and the BBL were applied to excite the CQDs, and the phase delay was tuned to control the wavelength shift of the spectrum. The experiments were conducted in an open environment at room temperature (25 ± 2 °C) in the lab.

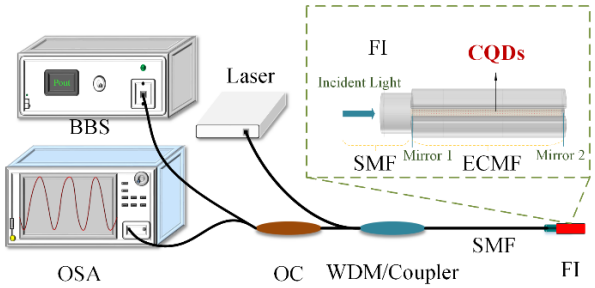

Fig. 2. Experimental setup for colloidal quantum dot -based light control FI. Two laser wavelengths of 1550 nm and 980 nm were used in the experiment to examine the two types of CQDs synthesized in the study. The CQDs were deposited along the exposed air hole in the ECMF.

3. Performance of light-controlled FI

We note that the phase difference introduced by the FI leads to the generation of an interference spectrum. Therefore, a wavelength shift should be observed when the phase is altered. The phase difference can be written as

$$\varphi = 2\pi n_{\text{eff}} L / \lambda \quad (1)$$

Optics EXPRESS

The L is the cavity length and in this work it equal to the length of the ECMF. The λ is the wavelength. The n_{eff} is the effective RI of optical mode propagated along the ECMF. The effective RI is related to the RI of the fiber and the RI of the CQD. The wavelength shift can be expressed as

$$W_{\text{shift}} = 2\Delta n_{\text{eff}} \Delta\lambda L / \lambda \tag{2}$$

The $\Delta\lambda$ is the FSR of the interference fringes and the Δn_{eff} is the effective RI change. In our study, the length and the RI of the fiber are constant since the temperature is stable. Therefore, the wavelength shift can be only observed when the RI of the CQD is altered.

The PbS CQD was synthesized in our experiments since the size-relevant absorption wavelength of PbS CQD can be controlled in the low-attenuation region in the fiber. To analyze the working principle of the light-controlled FI, two kinds of CQDs were prepared in our study, whose absorption wavelengths were 1180 nm and 1580 nm.

We first confirm that the phase factor in the FI fabricated by the ECMF without CQD deposition was power-independent. The results of our "blank test" (ECMF without CQD deposition) are shown in Fig. 3(a). A BBL source was applied to the FI with the source power ranging from 10 to 40 mW. The power only changed the intensity of the spectrum, and no wavelength shift was observed. These results indicate that the wavelength shift of the FI without CQD deposition was power-independent as expected.

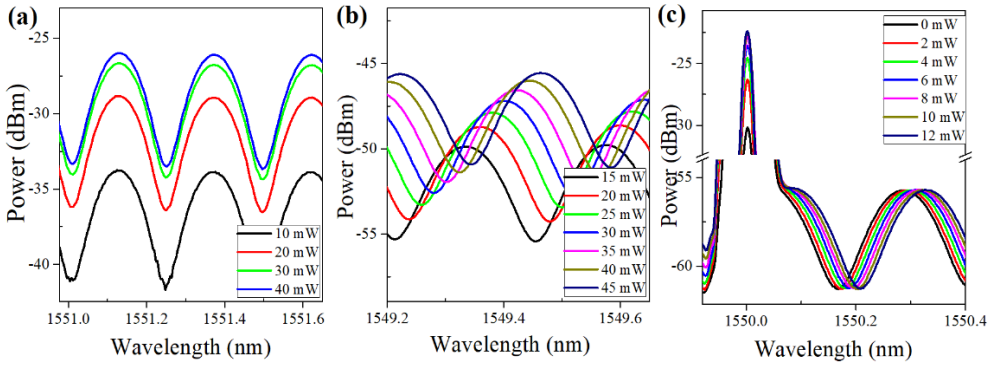

Fig. 3. Experiment result of the FI structure and the 1580-nm-absorption-wavelength CQD-based device controlled by C-band light. (a) Power response of "blank" structure without the quantum dots when injected by the BBL. With change in the BBL power, only an intensity change (no phase change) is observed. (b) FI transmission spectrum as a function of BBL power. (c) FI transmission spectrum power as a function of SSL power with the BBL being used to at constant power to observe the optical spectrum.

3.1 Results of 1580-nm-absorption-wavelength CQD-based device

The size-relevant absorption wavelength of the PbS CQDs was around 1580 nm, corresponding to a band gap of 0.785 eV. Thus, any incoming photon energy beyond 0.785 eV can excite the electrons in the valence band (VB) to the conduction band (CB), hence light with wavelengths shorter than 1580 nm can be absorbed by the CQDs. Owing to the low loss of C-band (1530-1565 nm) light in SMF (typically 0.2 dB/km), it can be transmitted for a long distance and acts as the remote control light of the 1580-nm CQD based devices.

A BBL source was first applied as the control light source. In the experiment, the light power was measured at the light source, and then this input power was increased in steps of 5 mW to record the spectra for each input power. The experimental results are shown in Fig. 3(b). From the figure, an evident red shift of the wavelength can be observed as the control light power increases. These results indicate that the RI of the CQD was altered during the experiment. We observe that the FSR of the spectrum is 0.24 nm, corresponding to the ECMF length of 3.4 mm, and the extinction ratio is 18 dB. In order to evaluate the performance of

Optics EXPRESS

the light-controlled FI, we defined the parameter of power sensitivity as the ratio of the wavelength shift to the control power. The sensitivity in the 1580-nm CQD FI controlled by BBL was 4.2 pm/W.

Next, a single-wavelength laser (SWL, Oclaro, LC96AA74-20R) with center wavelength at 1550nm was employed as control light source in the experiment to determine if the SWL could be utilized as the excitation light source. In this experiment, the BBL was stabilized at 30 mW to observe the spectra of the FI while the SWL was used to induce and control wavelength shift of the spectra. A coupler was used to couple the SWL with the BBL Subsequently, this light was transmitted to the FI. The total power including the SWL and BBL was measured at the output of the coupler. Since the power of the BBL was constant and the power of the SWL increased, the change in the total power equaled the change in the SWL control light power. The spectra were recorded for each 2-mW step increment of the control power; the corresponding experimental results are illustrated in Fig. 3(c). A change in power can easily be observed in the left portion of the spectrum, while a red shift of the wavelength can be observed in the right portion. The sensitivity was 3.6 pm/mW.

A wavelength shift could be observed in both the SWL and the BBL experiments. Importantly, we note that the control power was the key factor underlying the RI change and that the wavelength shift of the fiber filter exhibits a linear relationship with the control power. Our experiments prove that a laser operating at ~1550 nm can be used to remotely control passive fiber devices with several mWs of power. Besides, the sensitivity corresponding to the BBL control power experiment was bigger than that of the SWL experiment in the 1580-nm-CQD-deposited devices, which means that the RI change with the BBL as the control power is larger than that with the SWL. A reasonable assumption to explain this difference is that the RI change in the CQD is associated with the number of excited electrons. Although the BBL and the SWL are set to the same power, the photon energies are different; therefore, the number of photoelectrons is different.

3.2. Results of 1180-nm-absorption-wavelength CQD-based device

The absorption wavelength of the CQDs plays an important role in the functioning of our proposed devices. To understand the operating principle of the proposed device, we fabricated a new FI deposited with PbS CQDs with an absorption wavelength of ~1180 nm. The band gap of the 1180-nm CQD was 1.05 eV. The photon energy of the C-band laser was less than the CQD band gap, which meant that the laser wavelength could not be absorbed by the CQD. In this experiment, both the 1550nm SWL and the BBL were used to activate the 1180-nm CQD-deposited fiber filter. As a reference, a SWL with 980-nm wavelength (photon energy of 1.27 eV, higher than the band gap of the 1180-nm CQD) was also used to activate the FI to verify if CQDs with different sizes could still act as functional materials for light control.

The experimental results with the use of the BBL as control power are shown in Fig. 4(a), and the use of 1550 nm SWL was shown in Fig. 4(b). In this case, the FSR was 2.4 nm, almost the same as that obtained with the 1580-nm CQD-filmed fiber device. However, no wavelength shift was observed under the same experimental conditions; the C-band light did not have the ability to change the RI of the 1180-nm CQD. The 980-nm SWL control light experimental results are shown in Fig. 4(c). The relative power of the 980-nm SWL was measured at the output of the WDM. The experimental setup was identical to that of the 1550-nm SWL experiment mentioned previously. The control power of the 980-nm SWL was increased in steps of 2 mW, and a red shift of the wavelength was observed in the experiment, thereby indicating that the RI of the 1180-nm CQD was altered by the 980-nm light. The wavelength sensitivity of the 1180-nm CQD deposited FI was 4.6 nm/mW in the experiment. Correspondingly the effective RI change of the fiber was calculated as 5×10^{-6}/mW.

This experiment indicates that the wavelength of the control light is another factor that can be used to control the CQD RI. Light whose photon energy exceeds the band gap can be absorbed by the CQD, thereby resulting in change in the CQD RI, and vice versa. This

Optics EXPRESS

property can be used to assign the control wavelength in light-controlled devices. The control light wavelength should be set to a value less than the CQD absorption wavelength so that it can be absorbed to vary the CQD RI. The operating wavelength should be designed to be greater than the CQD absorption wavelength to ensure that it is not absorbed by the CQD.

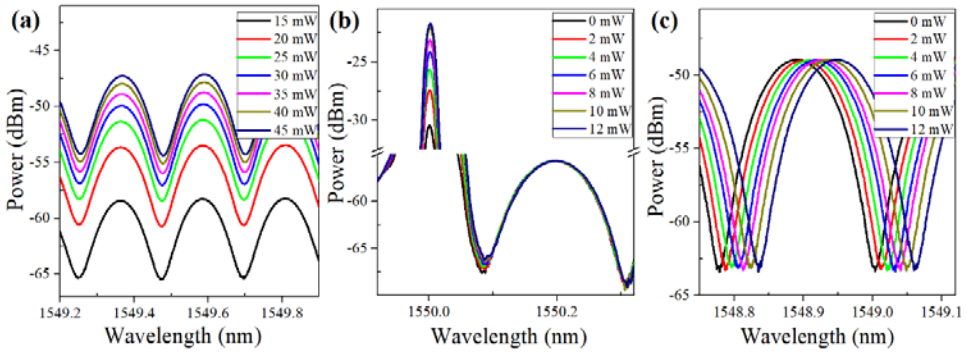

Fig. 4. Light control experiment with 1180-nm quantum dots deposited FI. (a) FI transmission spectrum as a function of BBL power. The spectra exhibit no wavelength shift with the control power changing from 15 to 45 mW. (b) FI transmission spectrum power as a function of SSL power with the BBL being used to at constant power to observe the optical spectrum. The spectra exhibit no wavelength shift with the control power of 1550 nm changing from 0 to 12 mW. (c) Light control experimental result for 1180-nm quantum dots with the control light wavelength of 980 nm. An obvious red shift of the wavelength is observed, which confirms that the 980-nm laser changes the refractive index of the CQDs.

3.3. Recovery property of fabricated device

An important aspect of optical elements (particularly those used in communication systems) is their stability. In this work, we designed an experiment to investigate the recovery property of the CQD-sensitized light-controlled FI. In this experiment, the BBL output was transmitted to the 1580-nm PbS-CQD sensitized fiber device and its power was increased from 15 to 50 mW in steps of of 5 mW (steps 1 to 7). Subsequently, the light power was decreased from 50 to 15 mW in steps 7 to 13, and the spectrum was recorded at every step (Fig. 5). The characteristic of the 1580-nm PbS CQD-deposited fiber device has been discussed above, and it is known that the BBL can excite the 1580-nm PbS CQD to exhibit an RI change. Further, it was observed in the experiment that spectrum of the fiber filter can return to the original position (“recovery”) as the light control power decreases. The result indicates the wavelength shift is independent of the energy accumulation. The position of the spectrum is one-to-one correspondence to each control power. Therefore, the device is believed to be stable and recoverable.

The linear relation and the repeatable experimental results suggest the photoelectron density change in the CQD film, not the temperature variation, was the reason for the RI change of the CQD. Further, the results also indicate that the laser power is the key control factor underlying the CQD RI change for a certain wavelength of light. When incident light is absorbed by the CQD, the number of available photoexcited electrons is the result of a dynamic equilibrium between their generation and recombination. Therefore, the concentration of the electrons, the RI change, and the wavelength shift are constant for a given control power.

Optics EXPRESS

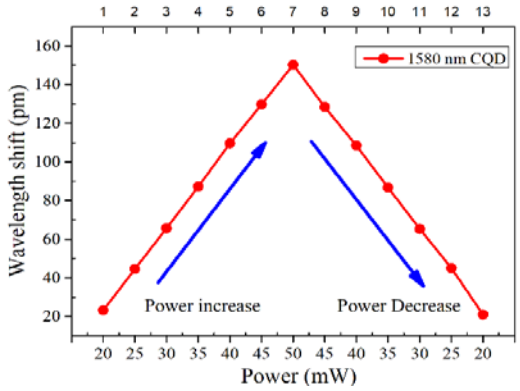

Fig. 5. Results of experiment to investigate the recovery property of the fabricated FI deposited with 1580-nm CQD. The power of the BBL source is increased from 15 to 50 mW in steps of 5 mW from step 1 to step 7. Subsequently, the BBL power is decreased from 50 to 15 mW in steps 7 to 13. Every measuring point is stabilized for 5 min.

3.4. Operation principle of the device

The observed wavelength shift is attributed to the CQD RI change, and the RI is the parameter that represents the polarization characteristics of CQDs. We proposed the photoexcitation dynamics theory that photoexcited electrons change the polarization in CQDs, and as a result, the RI of the CQDs is altered as a function of the excitation light. Although several studies have researched the carrier-density-based physical parameter change in CQDs [31], very few studies have investigated the optical property of CQD RI change under light excitation. Here, we calculate the CQD RI change and investigate the relation between the light power and the RI change. As per the Drude model, the dielectric function can be expressed as

$$\tilde{\varepsilon} = \varepsilon_b - N \times \frac{q^2}{\varepsilon_0 m_e (\omega^2 + \mathrm{j}\omega\tau^{-1})} \tag{3}$$

Here, ε_b denotes the ground dielectric constant, N the density of excited electrons per volume, q the elementary charge, ε_0 the vacuum permittivity, m_e the effective mass, ω the angular frequency, and τ the carrier lifetime. For the wavelength (around ~1550nm) utilized in the communication system, the N need to be biased at 10^{18}~10^{19} cm^{-3} to observe significant RI change. In CQD, the electrons are confined in a small volume due to the quantum confinement effect. Therefore, for the CQD, the excited electron charge density can be calculated as

$$N = x \times \alpha I \tau / V \tag{4}$$

where x is the CQD amount in volume V, α represents the absorption coefficient, I the light power applied to the CQD. If a single CQD volume was assumed to be V_{QD}. Then we can get an approximation relation between the V and V_{QD}.

$$V \approx x \times V_{QD} \tag{5}$$

Subsequently, we can calculate the RI as

$$n = \sqrt{\left(\left(\varepsilon'^2 + \varepsilon''^2 \right)^{1/2} + \varepsilon' \right) / 2} \tag{6}$$

Parameters ε' and ε'' denote the real and imaginary components of the dielectric constant. For an initial light with normalized intensity I_0, we assume that the average excited electron was 1

Optics EXPRESS

in every CQD. Next, if we assume the α and the τ was constant under the light illumination, the RI change can be calculated as the light intensity increases to I, as illustrated in Fig. 6. Two facts can be inferred from the calculation. The first one is that the RI was decreased when the light power was enhanced. The decreasing of RI is the reason for the red shift of the spectrum observed in experiment. The second is that the RI change of different-sized CQDs is linear with respect to the light power applied to the FI, and the linear relation agrees with the observed experimental data. In general, the electron concentration in nanomaterials can easily be biased to a large value owing to the quantum confinement effect of the CQD in which the electrons are constrained to several nanometers. Therefore, the required light power could be of order of mW while that for the bulk material is of the order of watts in the electronic equilibrium state.

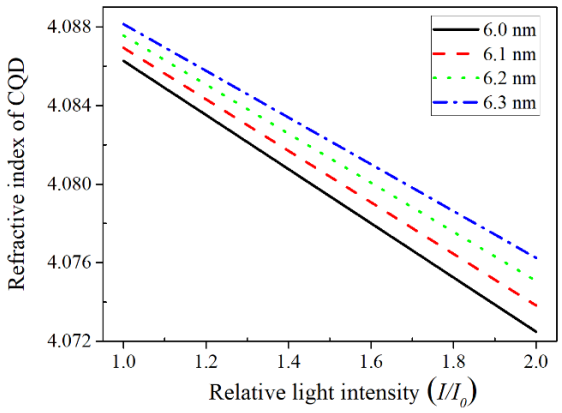

Fig. 6. Calculation result of RI at 1550 nm for various CQD sizes as a function of the relative light intensity absorbed by the CQD. The relationship between the RI change and the number of electrons is linear.

4. Light-controlled CQD deposited FI in 12.5-Gbps OOK transmission system

In the directly modulated laser (DML) based intensity modulated direct detection (IMDD) fiber communication systems, the spectrum broadening becomes a serious problem when high-speed signals are modulated. Further, chirp management and dispersion compensation become very important. One of the approaches to solve this problem involves “shaving” the long-wavelength part of the broadened pulse to perform pulse compression thus improve the quality of the signals [32]. By using the light-controlled CQD-sensitized FI as a spectrum shaper in communication systems, flexible and efficient chirp management and dispersion compensation in high-speed DML system can be achieved.

Our experimental setup is illustrated in Fig. 7(a). Since the transmission wavelength of the communication system was around 1550 nm, which could be absorbed by the 1580 nm CQD, the 1180-nm CQD was utilized in the experiment to avoid any interference from the transmission light in the LCFF. A 980-nm laser was coupled to the LCFF by means of a WDM. The output power of the 980-nm laser was set by adjusting the applied electric current, and thus, the operation state of the LCFF could be precisely controlled. The working wavelength of the DML was 1549.4 nm, and it was biased at 300 mA to obtain the optimal performance. The pulses from the DML were shaped by the LCFF and then amplified by an erbium-doped fiber amplifier (EDFA). The resulting signal was detected by an avalanche photodiode (APD), and the bit error rate (BER) was calculated offline using the records of a digital storage oscilloscope (DSO). For the back-to-back (B2B) experiment, the LCFF signal from the DML was directly transmitted to a variable optical attenuator (VOA) to fix the power before the EDFA instead of transmission in 50 km standard single mode fibers (SSMFs).

Optics EXPRESS

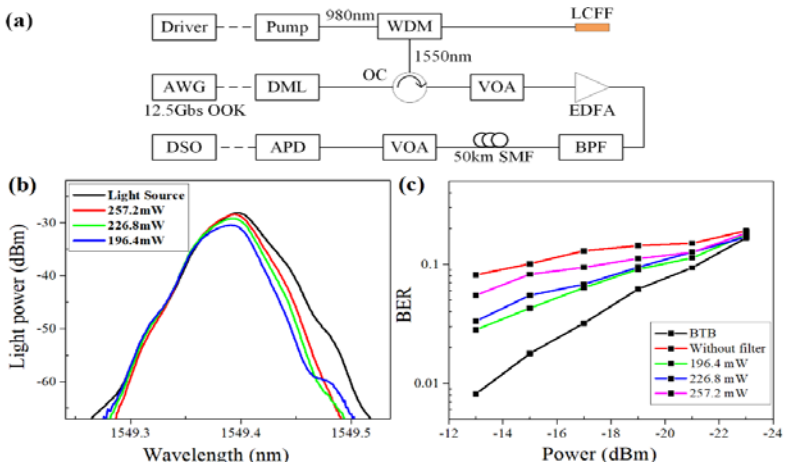

Fig. 7. Experiment result of the CQD enabled device in transmission system. (a) Experimental setup for 50-km 12.5-Gbps OOK signal communication. (b) Optical spectrum of the DML after filtered by the LCFF. The black curve denotes the spectrum of the "operating" light from the DML after modulation by the 12.5-Gbps OOK signal. Corresponding to the different pump powers, the output wavelength curves are indicated in pink, green, and blue. (c) BER curves of the system for various input powers. The back-to-back (BTB in the figure) experiment result is indicated by the black curve, while that for the system without the LCFF is indicated by the red curve and it was directly transmitted in 50-km SSMF. By tuning the control power, the LCFF can be used to shift the spectrum to the position where the long-wavelength portion of the light source is filtered.

In the experiment, the current of the 980-nm laser was tuned to adjust the positions of the peaks and troughs of the filter. Three positions of the filter at which the signal quality was high were determined. The output powers of the 980-nm control laser were 196.4 mW, 226.8 mW, and 257.2 mW. As shown in Fig. 7(b), the power of the long-wavelength portion reduces when compared with that of the light source after the filter. In this manner, the chirp and dispersion induced inter-symbol-interference (ISI) can be suppressed. The BER curves are shown in Fig. 7(c). The B2B experiment results exhibit the lowest BER at every received power value at the APD, while the system without the LCFF shows the poorest BER performance. Further, we note from the figure that the position of the LCFF spectrum changes upon tuning the control power. The signal quality can be enhanced if the long-wavelength portion of the pulse is filtered. The optimal position of the LCFF spectrum, corresponding to the least BER, could be determined by adjusting the control power. Importantly, the overall signal quality and system performance were found to improve with application of our light-control device.

5. Conclusion

In summary, we propose to use the solution-processed CQDs and ECMF to fabricate light-controlled optical devices. The FI sensitized by two types of PbS CQDs was demonstrated as an example. Table 1 present the light source setup and the experiment sensitivity for different CQDs. We revealed that the CQD RI change exhibits a linear relationship with the photoexcited electron concentration. The experimental results illustrated that only light with wavelengths absorbed by the CQD enables functioning of the FI. In addition, the incident light power shows a linear relationship with the RI change in the fiber devices, in consistency with the theoretical model. For actual optical-fiber-communication applications, we used a 980-nm laser as the control light source for a CQD-sensitized LCFF and a 1550-nm laser for communication signals. The CQDs with a central absorption wavelength of ~1180 nm were used in the fiber filter such that the control light could be absorbed to tune the LCFF, and importantly, the communication signals could be transmitted transparently. The proposed

Optics EXPRESS

optical fiber elements were then employed in a 50-km-long SMF communication system with a 12.5-Gbps OOK signal modulated for chirp management and dispersion compensation. The results indicate that the signal quality exhibited significant improvement upon suitably optimizing the CQD-deposited LCFF.

To the best of our knowledge, the light control devices based on RI change in CQD induced by light absorption was not reported before this work. Any optical fiber structures in which the light could interact with CQD can be used to design light controllable devices, such as micro-nano fiber, tilted grating, long period fiber grating, planar waveguide and so on. In principle, the liquid state functional materials (such as liquid crystal, alcohol, or magneto fluid) based fiber devices are unstable. While, the solid state materials (zirconate titanate, semiconductors, or metals) are difficult to operate at the micro scale of fiber structure and combine with silica fiber. Under these considerations, the CQD based fiber devices are anticipated inherently more robust. The light absorption power required to change the RI of the CQDs was of the order of mW at electronic equilibrium, which value is significantly smaller than that of bulk materials (of the order of watts). The CQD-based functional devices are power-efficient and promising for the application in flexible optical fiber communication systems. It should be noted that the speed of RI change of CQD was restricted by the lifetime of photoelectrons. Since the CQD is a highly tunable material, the lifetime can be adjusted by many methods, such as using different compositions, tuning the defects for fast recombination, and researching the annealing progress for crystallization. The ultra-fast optical devices using CQDs will be explored in the future.

Table 1. Light source setup for different type of CQD in the experiment.

CQD type	BBL source 1525-1575 nm power range (mW)	SWL source 1550nm power range (mW)	SWL source 980nm power range (mW)	Sensitivity (pm/mW)	Figure
none	10-40	-	-	none	3a
1580nm	15-45	-	-	4.2	3b
1580nm	30	0-12	-	3.6	3c
1580nm	15-50	-	-	*4.3*	5
1580nm	50-15	-	-	*4.3*	5
1180nm	15-45	-	-	none	4a
1180nm	30	0-12	-	none	4b
1180nm	30	-	0-12	4.6	4c,7

Funding

National Natural Science Foundation of China (61331010, 61722108); National Key Research & Development Program of China (2016YFC0201300); Key Projects of Hubei Natural Science Fund (2015CFA055).

Acknowledgments

The funding from ARC Centre of Excellence for Nanoscale BioPhotonics is acknowledged. This work was performed in part at the Optofab node of the Australian National Fabrication Facility (ANFF) utilizing Commonwealth and South Australian State Government funding. We wish to thank Stephen Warren-Smith and Alastair Dowler from the University of Adelaide for fiber fabrication. We thank the analytical and testing center of HUST for the characterization support.